Volume 20
Number 48
28 December 2024
Pages 9515–9696

Soft Matter

rsc.li/soft-matter-journal

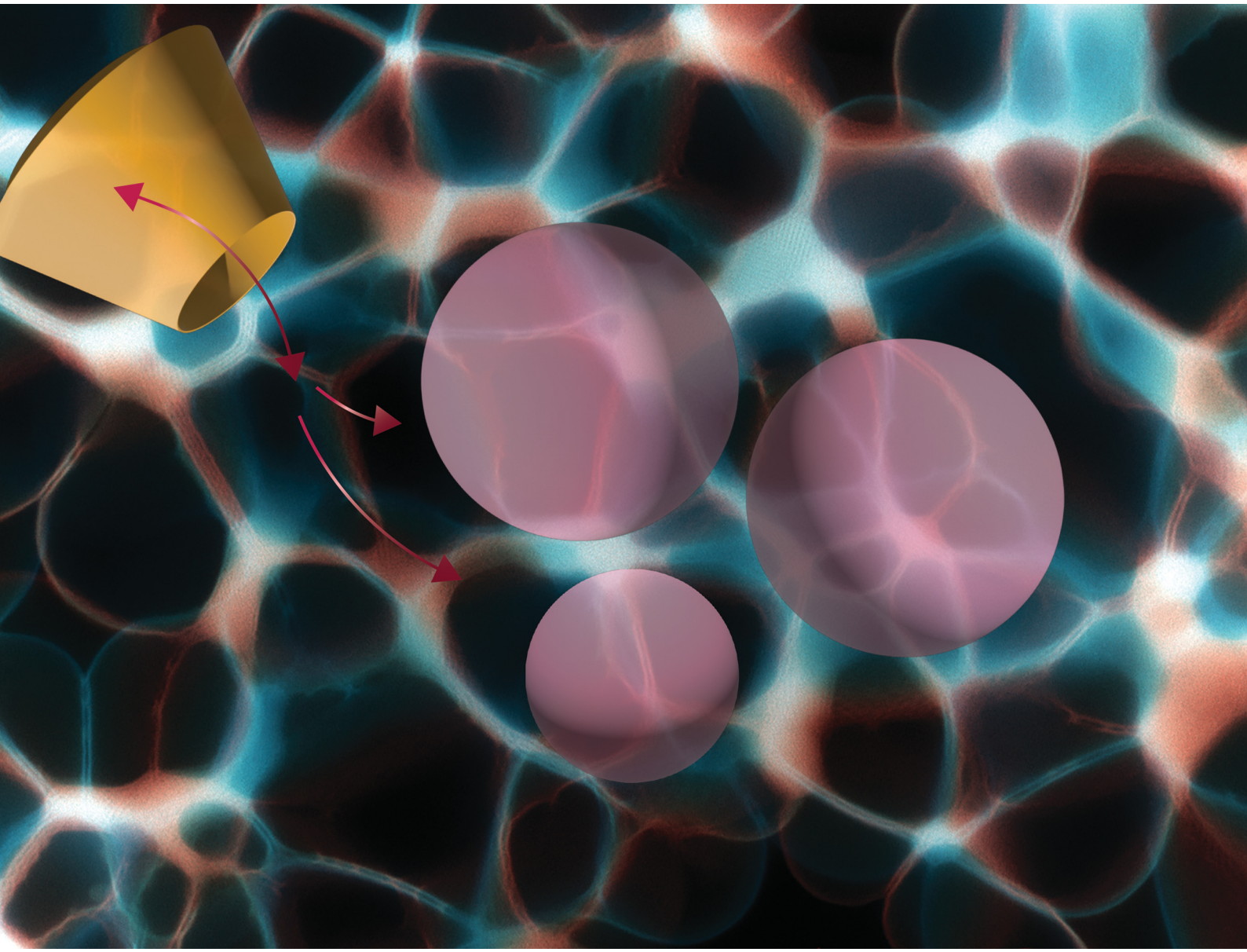

ISSN 1744-6848

ROYAL SOCIETY OF CHEMISTRY

PAPER
Alexis Cooper and Anand Bala Subramaniam
Ultrahigh yields of giant vesicles obtained through mesophase evolution and breakup

Soft Matter

PAPER

View Article Online
View Journal | View Issue

Cite this: *Soft Matter*, 2024, **20**, 9547

Ultrahigh yields of giant vesicles obtained through mesophase evolution and breakup†

Alexis Cooper [a] and Anand Bala Subramaniam *[b]

Received 19th September 2024,
Accepted 13th November 2024

DOI: 10.1039/d4sm01109k

rsc.li/soft-matter-journal

Self-assembly of dry amphiphilic lipid films on surfaces upon hydration is a crucial step in the formation of cell-like giant unilamellar vesicles (GUVs). GUVs are useful as biophysical models, as soft materials, as chassis for bottom-up synthetic biology, and in biomedical applications. Here *via* combined quantitative measurements of the molar yield and distributions of sizes and high-resolution imaging of the evolution of thin lipid films on surfaces, we report the discovery of a previously unknown pathway of lipid self-assembly which can lead to ultrahigh yields of GUVs of >50%. This yield is about 60% higher than any GUV yield reported to date. The "shear-induced fragmentation" pathway occurs in membranes containing 3 mol% of the poly(ethylene glycol) modified lipid PEG2000-DSPE (1,2-distearoyl-*sn*-glycero-3-phosphoethanolamine-*N*-[methoxy(polyethylene glycol)-2000]), when a lipid-dense foam-like mesophase forms upon hydration. The membranes in the mesophase fragment and close to form GUVs upon application of fluid shear. Experiments with varying mol% of PEG2000-DSPE and with lipids with partial molecular similarity to PEG2000-DSPE show that ultrahigh yields are only achievable under conditions where the lipid-dense mesophase forms. The increased yield of GUVs compared to mixtures without PEG2000-DSPE was general to flat supporting surfaces such as stainless steel sheets and to various lipid mixtures. In addition to increasing their accessibility as soft materials, these results demonstrate a route to obtaining ultrahigh yields of cell-sized liposomes using longstanding clinically-approved lipid formulations that could be useful for biomedical applications.

1 Introduction

Giant unilamellar vesicles (GUVs), single-walled phospholipid vesicles with diameters ≥ 1 μm, are useful for biomimetic and bioinspired experiments since they can reproduce key characteristics of cellular membranes such as their size, semi-permeability, mechanical and surface properties in an experimentally tractable minimal model.[1–4] Due to their ability to mimic these key characteristics of cells, GUVs show promise for applications in soft matter,[5–8] biomedicine,[9–11] and bottom-up synthetic biology.[12–14]

GUVs are routinely obtained using thin film hydration, which are a class of methods that involves hydrating dry thin lipid films with low ionic strength aqueous solutions.[15–18] We recently reported an analytical framework to quantify the distribution of diameters and molar yields of populations of GUVs using sedimentation, high-resolution confocal microscopy, and large data set image analysis.[16] Thin film hydration results in a wide distribution of GUV diameters ranging from 1 μm to 100 μm. To allow statistical comparison of the yields of polydisperse populations of GUVs, we introduced the concept of the molar yield of GUVs. The molar yield, calculated from the diameters and counts of GUVs, measures the moles of lipid in the membranes of the population of harvested GUVs relative to the moles of lipids that was initially deposited on the surface.[16] The molar yield accounts for the quadratic dependence of the amount of lipid in a GUV membrane on the diameter of the GUV. Additionally, the molar yield has an analogy to chemical synthesis. The amount of lipid per unit area deposited onto the surface is the concentration of the reactant and the amount of lipid in the membranes of the harvested GUVs is the product. The molar yield, the counts, and the distribution of sizes allow for the interrogation of the effects of experimental variables on the assembly of GUVs.[16] By correlating the evolution of the film on the surface with quantitative measurements of the yield, we studied the effects of physicochemical parameters such as the geometry and chemical composition of the substrate used to support the lipid film,[16] the lipid composition,[15] the identity of assisting polymeric compounds,[15] the duration[19] and the temperature[15] of incubation, and the ionic strength of the

[a] *Department of Chemistry and Biochemistry, University of California, Merced, CA 95343, USA*
[b] *Department of Bioengineering, University of California, Merced, CA 95343, USA. E-mail: asubramaniam@ucmerced.edu*

† Electronic supplementary information (ESI) available: Representative images of harvested GUVs, original orthogonal Z-stack reconstructions, and histograms of GUV size distributions. Tables showing: F and *p*-values of statistical tests. See DOI: https://doi.org/10.1039/d4sm01109k

hydrating solution.[15] Depending on the conditions of assembly, mean GUV molar yields ranged from "low", 0.3–4.9%, "moderate", 5–19.9%, and "high", 20–40%.

Surfaces composed of enmeshed nanocylinders, such as the nanocellulose paper used in the PAPYRUS method, Paper-Abetted amPhiphile hYdRation in aqUeous Solutions, resulted in a higher yield of GUVs compared to the flat surfaces used in the gentle hydration and electroformation methods.[16,19] This result was explained by comparing the free energy of the lipids configured as a spherical bud *versus* a bilayer remaining on the substrate. Calculations showed that the free energy change to form a bud can be negative for bilayers on nanocylinders, while the free energy change to form a bud is always positive for bilayers on flat surfaces. Once formed, merging of the buds with each other to reduce the total number of buds reduces the elastic energy of the system. A hypothetical pathway involving both budding and merging provides an energetically favorable path for bilayers on nanoscale cylinders to form large GUV-sized buds. In contrast, the path on flat surfaces requires the input of energy.[16] A similar free energy argument shows that the dissolution of partially soluble polymers exerts an osmotic pressure that can balance the increased adhesion between bilayers due to the screening of electrostatic charges in salty solutions. The osmotic pressure contribution lowers the free energy of budding, thus resulting in high yields of GUVs in salty solutions.[15]

In this work, we investigate the effects of adding 0.1–10 mol% of poly(ethylene glycol) modified (PEGylated) lipids on the pathway of assembly of GUVs composed of the zwitterionic lipid DOPC (1,2-dioleoyl-*sn*-glycero-3-phosphocholine) through the PAPYRUS, gentle hydration and electroformation methods.[16,18–22] PEG2000-DSPE (1,2-distearoyl-*sn*-glycero-3-phosphoethanolamine-*N*-[methoxy(polyethylene glycol)-2000]) has a long history of use in clinical lipid formulations because it improves the circulation lifetime by reducing opsonization of nano-sized liposomes and lipid nanoparticles by serum proteins.[23–28] For applications involving GUVs, PEGylated lipids are used to prevent the aggregation of GUVs in salty solutions. These lipids have been used in GUVs designed to target and induce apoptosis in leukemia cells,[11] deliver intracellular cargo,[29] drive differentiation of neuronal cells,[30] trigger DNA-mediated fusion,[31] and augment the functionality of bioprinted artificial tissues.[10] They are also used in GUVs that encapsulate cytoskeletal proteins[14] and cell-free gene expression mixtures,[32] and in GUVs used in test-strip based sensing.[33] PEG2000-DSPE consists of an uncharged hydrophilic polymer of 45 repeating ethylene glycol monomer units with an average molecular weight of 2000 g mol^{-1} that is covalently attached to the headgroup of the phospholipid DSPE. The utility of PEG2000-DPSE for applications has led to many experimental and theoretical investigations of its effects on the physicochemical properties of membranes such as intermembrane forces,[34–37] phase behavior,[38–40] mechanical properties,[40–45] permeability,[44,46–48] and protein adsorption.[48,49] Model systems that have been investigated include oriented multilayers,[26,36,37] supported lipid bilayers,[26,36,50] small unilamellar liposomes,[46,47] GUVs,[44] multilamellar vesicles,[34,35,37,39] and Langmuir monolayers.[51] Most studies employ lipid membranes in the gel-phase.[26,34–36,39,44,47,49,51] Comparatively less is known about the effects of PEGylated lipids on the pathway of assembly of GUVs[52,53] or in fluid phase membranes,[37,46] despite the wide use of GUVs with fluid phase membranes in experiments.[1–3,7,14]

We find, unexpectedly given previous results,[16,19] that we can obtain yields of $>50\%$ of GUVs when the lipid mixture contained 3 mol% PEG2000-DSPE using the gentle hydration method on flat glass surfaces in low salt solutions. This yield is $\sim$175% higher than the yield of GUVs obtained using pure DOPC through the gentle hydration method. The yield is the highest that has been measured thus far, leading us to add a classification of "ultrahigh" for yields $>45\%$ and to extend the upper range of "high" molar yields to 44.9%. Interestingly, obtaining this ultrahigh yield was specific to the gentle hydration method and only when the mixture had 3 mol% PEG2000-DSPE. We find that there was no difference in GUV yields between the mixture containing 3 mol% PEG2000-DSPE and pure DOPC obtained using the PAPYRUS method. Furthermore, performing the gentle hydration method using mixtures with other mol percents of PEG2000-DSPE resulted in yields that ranged from 16–30%.

High resolution three-dimensional confocal microscopy images of the hydrated lipid films on the surface show that the DOPC + 3 mol% PEG2000-DSPE lipid mixture rapidly forms a lipid-dense foam-like mesophase. Although a qualitatively similar mesophase forms with a DOPC + 5 mol% PEG2000-DSPE lipid mixture, the lipid content of the mesophase was low and micelles were present in the solution. There was no mesophase for the other mol percents of PEG2000-DSPE or on the surface of nanocellulose paper. Instead, the lipid assembles into surface-attached buds for mixtures containing $\leq$1 mol% of PEG2000-DSPE and sparse free-floating clusters of GUVs and micelles for mixtures containing 10 mol% PEG2000-DSPE. Importantly, we find that different configurations of the lipid on the surface can lead to similar yields of GUVs upon harvesting.

To understand the physical interactions that promote the formation of the foam-like mesophase, we use lipids with partial molecular similarity to PEG2000-DSPE. We find that use of lipids that do not have both a charged headgroup and a covalently attached PEG2000 chain did not result in the formation of the foam-like mesophase nor did it result in GUV yields different from pure DOPC. Additionally, we find that screening of the charge on PEG2000-DSPE by using solutions with dissolved salts prevents the formation of the foam-like mesophase and results in a dramatic drop in GUV yields. We also show that an increase in GUV yield upon addition of 3 mol% PEG2000-DSPE appears general to other lipid mixtures and other flat surfaces.

Guided by these results, we propose a mechanism of assembly of GUVs when the lipid mixture contains 3 to 5 mol% PEG2000-DSPE. During harvesting with a pipette, the lamellar membranes in the foam-like mesophase fragments due to fluid shear and self-close to form GUVs. This "shear-induced

fragmentation'' of the mesophase is an alternate, previously unrecognized, pathway for forming GUVs with fluid phase membranes containing PEG2000-DSPE that can lead to ultra-high yields.

2 Materials and methods

2.1 Chemicals

We purchased sucrose (BioXtra grade, purity ≥ 99.5%), glucose (BioXtra grade, purity ≥ 99.5%), sodium chloride (BioXtra grade, purity ≥ 99.5%) and casein from bovine milk (BioReagent grade) from Sigma-Aldrich (St. Louis, MO). We purchased chloroform (ACS grade, purity ≥ 99.8%, with 0.75% ethanol as preservative) Thermo Fisher Scientific (Waltham, MA). We obtained 18.2 MΩ ultrapure water from a Milli-Q® IQ 7000 Ultrapure Lab Water System (Burlington, MA). We purchased 1,2-dioleoyl-*sn*-glycero-3-phosphocholine (DOPC), 1,2-dipalmitoyl-*sn*-glycero-3-phosphocholine (DPPC), cholesterol (ovine wool), 1,2-dioleoyl-*sn*-glycero-3-phosphoethanolamine-*N*-(lissamine rhodamine B sulfonyl) (Rhod-PE), 23-(dipyrromethemeboron difluoride)-24-norcholesterol (TopFluor-Chol), 1,2-distearoyl-*sn*-glycero-3-phosphoethanolamine-*N*-[methoxy(polyethylene glycol)-2000] (PEG2000-DSPE), 1,2-distearoyl-*rac*-glycero-3-methoxypolyethylene glycol-2000 (PEG2000-DSG), 1,2-distearoyl-*sn*-glycero-3-phospho-(1'-*rac*-glycerol) (sodium salt) (DSPG), 1,2-distearoyl-*sn*-glycero-3-phosphoethanolamine (DSPE) from Avanti Polar Lipids, Inc. (Alabaster, AL).

2.2 Materials

We purchased premium plain glass microscope slides (75 mm × 25 mm, catalog number: 12-544-1) from Thermo Fisher Scientific (Waltham, MA). We purchased indium tin oxide (ITO) coated-glass slides (25 × 25 mm squares, surface resistivity of 8–12 Ω sq^{-1}) from Sigma-Aldrich (St. Louis, MO). We purchased a hole punch cutter (EK Tools) and acid free artist grade tracing paper from (Jack Richeson and Co. Inc) on Amazon. We purchased 0.001 inch (0.025 mm) thick stainless steel sheets from McMaster-Carr.

2.3 Cleaning of substrates

We clean all substrates as previously described.[16] We clean the glass slides and ITO-coated glass slides by sequentially sonicating for 10 minutes in acetone, 200 proof ethanol, and ultrapure water. We then dry the slides under a stream of ultrapure nitrogen to remove any visible water. We allow the slides to dry further in an oven set to 65 °C for a minimum of 2 hours.

We cut sheets of 0.001 inch (0.025 mm) thick stainless steel into rectangles of 75 mm × 25 mm using a glass slide as a template. We clean the stainless steel rectangles following the same procedure for cleaning glass slides.

We clean the tracing paper as previously described[16] by soaking the tracing paper in 100 mL of chloroform in a 500 mL glass beaker for 30 minutes with occasional manual agitation. We discard the chloroform and repeat the process with fresh chloroform. Then, we remove the tracing paper and leave the paper in the fume hood for 30 minutes. The substrates are then soaked in 500 mL of ultrapure water for 30 minutes. We discard the ultrapure water and repeat the process with fresh ultrapure water. The tracing paper is then placed on a clean sheet of aluminum foil and dried in a 65 °C oven for 2 hours.

2.4 Preparation of lipid stocks

Lipid mixtures were prepared as previously described with minor adaptations.[15,16,19] We prepared working solutions of DOPC with 0, 0.1, 1, 3, or 10 mol% PEG2000-DSPE and 0.5 mol% TopFluor-Chol and DOPC with 3 mol% each of DSPE, PEG2000-DSG, or DSPG and 0.5 mol% TopFluor-Chol. The mol% of DOPC was adjusted to accommodate the minority lipids. For phase separating GUVs, we created working solutions of DOPC/DPPC/Cholesterol/PEG2000-DSPE/Rhodamine-DOPE/TopFluor-Chol at 34.5/34.5/27.5/3/0.25/0.25 mol%, and DOPC/DPPC/Cholesterol/Rhodamine-DOPE/TopFluor-Chol at 36/36/27.5/0.25/0.25 mol%. All working solutions had a concentration of 1 mg mL^{-1}. The lipid solutions were stored in clean glass vials with Teflon lined caps, purged with argon to avoid lipid oxidation, and stored in a −20 °C freezer. Lipid solutions were used within 7 days of preparation.

2.5 Deposition of lipids

To ensure that the nominal surface concentration remained constant, we deposited 10 μL of the lipid working solution over a circular area with a diameter of 9.5 mm. For application on glass slides and ITO-coated glass slides, we punched three 3/8-inch diameter holes on the adhesive side of a 3 × 3 in Post-it® using a circular punch (EK Tools Circle Punch, 3/8 in.). The Post-it® was then affixed to the underside of the slides to create a removable and reusable template for spreading the lipid within a 9.6 mm diameter circular area. For assembly on tracing paper, we punched out a 9.6 mm diameter circular piece of tracing paper using a clean circular punch. For assembly on stainless steel sheets, we cut a template from paper using a circular punch and cut the stainless steel sheets to size using a pair of scissors. Lipids were deposited using a glass Hamilton syringe. Then, the lipid-coated substrates were placed in a standard laboratory vacuum desiccator for 1 hour to remove traces of chloroform.

2.6 Procedure for GUV assembly

For the gentle hydration method, circular poly(dimethyl)siloxane (PDMS) gaskets (inner diameter × height = 12 × 1 mm) were affixed to the glass slides around the dried lipid films to create a hydration chamber. We then added 150 μL of a solution of 100 mM sucrose and allowed the lipid films to hydrate for 1 hour at room temperature (22 °C). We do not place a coverslip on the chamber. To reduce evaporation, we enclosed the samples and a water-saturated Kimwipe in a 150 mm diameter Petri dish. The films were allowed to hydrate for 1 h. The gentle hydration method that we use here, first reported in ref. 16 employs flat glass microscope slides as substrates, lower lipid amounts spread as a thin layer, and smaller hydration volumes compared to other implementations of the gentle hydration method which required the inclusion of charged lipids, a

prehydration step with saturated water vapor, and long incubation times.[18,20–22] The hydrating lipid films are furthermore housed in custom built poly(dimethyl)siloxane (PDMS) chambers that allow reproducible conditions for micropipette-based harvesting.[16] These characteristics likely explains why the gentle hydration method using glass slides results in GUVs within a relatively short incubation time, and without requiring the addition of charged lipids or a prehydration step with saturated water vapor. The variation in the properties of populations of GUVs that result from different methodologies is receiving increasing attention in the field.[22]

We assemble phase-separated GUVs on a hotplate set to 45 °C to be above the transition temperature of DPPC (41 °C). A similar experimental setup to the procedure for assembly at room temperature resulted in the solution evaporating completely within 1 hour. We thus modified the hydration procedure by stacking three circular PDMS gaskets to create a tall hydration chamber (inner diameter × height = 12 × 3 mm) which allowed us to place a coverslip on the chamber without contacting the liquid. We found that when the coverslip contacted the liquid, removal of the coverslip results in fluid shear that affected reproducibility. We placed the sample in a closed 150 mm diameter Petri dish and set the dish on the hotplate for 1 minute to preheat. An average of ∼17 μL of liquid evaporates from the chamber. To account for evaporation, we add 167 μL of a solution of 90 mM sucrose. The solution was preheated to 45 °C before adding it into the hydration chamber. We then gently placed a coverslip on top of the tall PDMS chamber, placed a water-saturated Kimwipe in the dish, and replaced the lid on the Petri dish. The films were allowed to hydrate. After 1 h we removed the coverslips carefully to avoid the condensed water droplets from falling into the sample. We measured the osmolarity of a 20 μL aliquot using a freezing point depression multi-sample osmometer (Model 2020, Advanced Instruments, USA). Using this procedure, we obtained an average final sample volume of 150 ± 3 μL with an osmolarity of 100 ± 2 mM.

For the PAPYRUS method and gentle hydration method using the stainless steel sheets, the 9.5 mm diameter circles of the lipid-coated tracing paper or stainless steel sheets were placed in individual wells of a 48-well plate. 150 μL of a solution of 100 mM sucrose was then added to the wells and incubated for 1 hour at room temperature.

We follow previously established protocols to prepare GUVs using the electroformation method.[16,19,54,55] We use the same lipid deposition procedure as described in Section 2.5 to be consistent with the PAPYRUS and gentle hydration samples. Briefly, we affixed circular PDMS gaskets (inner diameter × height = 12 × 1 mm) around the dried lipid film on an ITO-coated glass slide to construct a barrier for hydration. We added 150 μL of 100 mM sucrose in ultrapure water and close the chamber using a second ITO-coated glass slide. The ITO-coated surfaces were then connected to the leads of a function generator (33120A, Agilent) using conductive copper tape. We applied a sinusoidal AC field at a frequency of 10 Hz and a field strength of 1.5 V mm^{-1} peak-to-peak for 2 hours.

The GUVs were harvested from all the surfaces by pipetting 100 μL of the solution up and down 6 times with a micropipette. On the 7th time, we fully aspirated the solution containing the GUVs and stored the solution in an Eppendorf tube. Aliquots were taken immediately for imaging. Each condition was performed $N = 3$ independent times.

2.7 Imaging of the harvested vesicles

Imaging was conducted as previously described.[16] Briefly, we imaged the GUVs in custom-made square poly(dimethylsiloxane) (PDMS) chambers with dimensions of 5.9 mm × 5.9 mm × 1 mm (length × width × height) affixed to a glass slide. We passivated the chambers with 1 mg mL^{-1} casein dissolved in PBS. We sedimented a 2 μL aliquot of the sucrose-filled GUVs in 58 μL of an isomolar solution of glucose in the imaging chamber. The GUVs are allowed to sediment for 3 hours, followed by imaging using an upright confocal laser scanning microscope (LSM 880, Axio Imager.Z2m, Zeiss, Germany), using a 488 nm argon laser and a 10× Plan-Apochromat objective with a numerical aperture of 0.45. The pinhole was 15.16 Airy Units to capture a slice thickness of 79.3 μm allowing imaging of GUVs with diameters from 1 μm to 150 μm. For phase separated vesicles, we captured dual channel images using a 488 nm argon laser and a 561 nm diode pumped solid state laser. The intensity and gain of the two channels were adjusted so that the mean intensity of both channels was similar. We imaged using an automated tile scan routine with autofocus (49 images [5951.35 μm × 5951.35 μm, (3212 pixels × 3212 pixels)]) to capture the entire area of the chamber. The routine focused 5 μm above the surface of the glass slide.

2.8 Image processing and calculation of yields

We processed and analyzed the images as previously described.[16,19] Briefly, we use a custom MATLAB (Mathworks Inc., Natick, MA) routine to segment fluorescent objects from the background and the *regionprops* function to obtain the diameters and pixel intensities of the objects. To distinguish GUVs from non-GUV lipid structures such as multilamellar vesicles and nanotubes, we selected objects based on the coefficient of variation (CV) of their intensity values. Objects that fell within 1.75 times the full width at half the maximum (FWHM) of the highest peak in the histogram of CV values were classified as GUVs. Additionally, objects that had more than 10% of their pixel values higher than 200 on a 256 intensity units scale were classified as not GUVs. We had previously confirmed that the number of GUVs identified using an α-hemolysin induced fluorescent dye leakage assay and the image analysis routine was similar.[56] The advantage of the image analysis routine compared to the dye leakage assay is that it allows a tractable workflow to collect the diameters of $n \sim 100\,000$ GUVs per repeat from multiple independent repeats. The large dataset allows statistical hypothesis testing to distinguish the effects of experimental variables on the distribution of sizes, yields, and fraction of non-GUV structures. Counts of GUVs were normalized per μg of lipid deposited on the substrate. We calculate the molar yield,

expressed as a percentage, using $Y = 100\left(\frac{2\pi m V_h}{N_A A_{hg} M V_{al}} \sum_{i=1}^{n} d_i^2\right)$. In this equation, m is the molecular weight of the lipid, V_h is the volume of the harvested GUV suspension, N_A is Avogadro's number, A_{hg} is the headgroup area of the lipid, M is the mass of lipid deposited on the surface, V_{al} is the volume of the aliquot in the imaging chamber, n is the number of GUVs in the imaging chamber, and d_i is the diameter of vesicle i.[19]

2.9 Statistical tests

All statistical tests were performed in MATLAB. We conduct student's *t*-tests to determine the statistical significance of any difference in magnitude between two independent group means. We conducted a one-way balanced analysis of variance (ANOVA) when comparing the significance of the difference in magnitude of means in experiments with more than two independent groups. If the ANOVA showed that the means were significantly different, we conducted a *post hoc* Tukey's honestly significant difference (HSD) to determine the statistical significance between pairs of means.

2.10 High resolution Z-stacks

We obtained confocal Z-stacks using a Plan-Apochromat 20× DIC M27 75 mm water dipping objective with a numerical aperture of 1.0. We took 189 slices of the hydrated lipid films at intervals of 0.9 μm starting from 4.5 μm into the surface of the substrate to 165.6 μm above the surface of the substrate. The images were 151.82 × 151.82 μm (1272 × 1272 pixels). Imaging locations were chosen to best represent the surface. Image processing was performed in FIJI.[57] We used the "*reslice*" function to obtain *x*–*z* slices from the confocal Z-stacks. We enhance the contrast of the *x*–*z* slices by using the "*enhance contrast* > *equalize histogram*" option in FIJI to show dim features and bright features. Non-contrast enhanced images are shown in the ESI.† We obtain *x*–*y* *z*-projections by summing the slices of the first 18 μm, starting 3 slices below the surface.

3 Results and discussion

3.1 The addition of 3 mol% PEG2000-DSPE to the lipid mixture affects the yield and distribution of sizes differently depending on the method of assembly

We assembled GUVs with membrane compositions of 99.5 : 0.5 mol% DOPC : TopFluor®-Chol and 97.5 : 3 : 0.5 mol% DOPC : PEG2000-DSPE : TopFluor®-Chol using the PAPYRUS and gentle hydration methods.[16] For brevity, we refer to these lipid compositions as "pure DOPC" and "DOPC + 3 mol% PEG2000-DSPE" respectively. TopFluor®-Chol is a fluorescent sterol used to visualize the lipid membranes through confocal fluorescence microscopy. Fig. 1a shows the molar yields of GUVs obtained using the PAPYRUS method and Fig. 1b shows the molar yield obtained using the gentle hydration method. Each bar is an

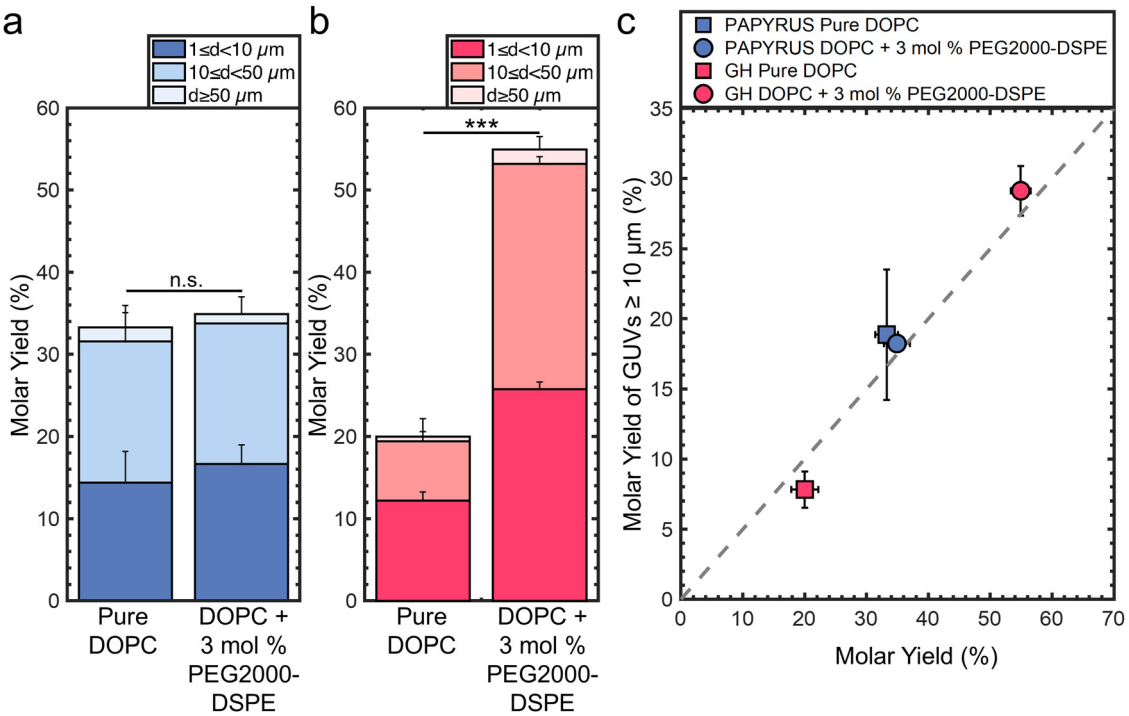

Fig. 1 Molar yields of GUVs from mixtures of pure DOPC and DOPC + 3 mol% PEG2000-DSPE. (a) Stacked bar plots showing the molar yield of GUVs obtained from the PAPYRUS method. (b) Stacked bar plots showing the molar yield of GUVs obtained from the gentle hydration (GH) method. The stacks show the percentage of the molar yield that is comprised of the size classifications as listed in the legend. (c) Scatter plot showing the molar yield of GUVs with diameters ≥ 10 μm *versus* the total molar yield. The grey dashed line indicates where half the lipid molecules are in GUVs with diameters ≥ 10 μm. Each data point is the average of n = 3 independent repeats. The error bars are one standard deviation from the mean. Statistical significance was determined using a student's *t*-test. *: $p < 0.05$, **: $p < 0.01$, ***: $p < 0.001$, n.s.: not significant.

average of $N = 3$ independent repeats and the error bars are one standard deviation from the mean. Following previous convention,[15,16,19] we divide the molar yield into GUVs with diameters, d, between 1 μm $\leq d <$ 10 μm, 10 μm $\leq d <$ 50 μm, and $d \geq$ 50 μm. The population classes were chosen because GUVs between 1 μm $\leq d <$ 10 μm are of the sizes of blood cells, intracellular organelles, and bacteria, and GUVs between 10 μm $\leq d <$ 50 μm are of the size of mammalian cells. We show representative images of the harvested GUVs and the histogram of diameters in ESI,† Fig. S1 and S2.

The mean yield of GUVs obtained using the PAPYRUS method is 33 ± 2% and 35 ± 2% for pure DOPC and DOPC + 3 mol% PEG2000-DSPE respectively (Fig. 1a). The 2% difference in the mean yields between these two lipid compositions was not statistically significant ($p = 0.451$). The mean yield of GUVs obtained using the gentle hydration method is 20 ± 2% and 55 ± 2% for pure DOPC and DOPC + 3 mol% PEG2000-DSPE respectively (Fig. 1b). The 35% difference in yield between the two lipid compositions was highly statistically significant ($p = 5.22 \times 10^{-5}$). Furthermore, the ∼20% difference in yield between DOPC + 3 mol% PEG2000-DSPE obtained using the gentle hydration method compared to the yields obtained using the PAPYRUS method for both compositions of lipid was highly statistically significant (both $p < 0.001$). Indeed, the 55% yield is the highest yield that has been measured to date for any thin film hydration method.[15,16,19]

We plot the yield of GUVs with $d \geq$ 10 μm (large GUVs) *versus* the total molar yield of GUVs to show the effects of the addition of 3 mol% PEG2000-DSPE on the distribution of sizes (Fig. 1c). The gray dashed line represents the boundary where half of the molar yield is from GUVs with $d \geq$ 10 μm. Data points that fall to the right of the line indicate that the sample has a smaller fraction of large GUVs compared to data points that fall to the left of the line. Consistent with previous results, GUVs with $d \geq$ 10 μm make up to ∼57% and 39% of the total yield for the lipid composition consisting of pure DOPC obtained using the PAPYRUS and gentle hydration methods.[16,19] In contrast, GUVs with $d \geq$ 10 μm make up to 52% and 53% of the total yield for the lipid composition consisting of DOPC + 3 mol% PEG2000-DSPE obtained using the PAPYRUS and gentle hydration methods.

These results show that the addition of 3 mol% PEG2000-DSPE to the lipid mixtures affects the yield and distribution of sizes differently depending on the method of assembly. For the PAPYRUS method, the addition of 3 mol% of PEG2000-DSPE to the lipid mixture does not affect the yield but decreases the fraction of GUVs with $d \geq$ 10 μm. For the gentle hydration method, the addition of 3 mol% PEG2000-DSPE to the lipid mixture increases both the yield and fraction of GUVs with $d \geq$ 10 μm.

We evaluate these results within the framework of the budding and merging (BNM) model for the assembly of GUVs.[16,19] eqn (1) and (2) gives the free energy for the formation of spherical buds of radius R_B from cylindrical bilayers, $\Delta E_{R_B,c}$, and disk-shaped flat bilayers, $\Delta E_{R_B,d}$. Bilayers on both surfaces are assumed to be continuous with no breaks prior to budding, Derivation of eqn (1) and (2) can be found in ref. 16.

$$\Delta E_{R_B,c} = \pi\kappa_B\left(8 - \frac{L_c}{R_c}\right) + 4\pi R_c\lambda - 2\pi R_c L_c\xi \quad (1)$$

$$\Delta E_{R_B,d} = 8\pi\kappa_B + 2\pi R_d\lambda - \pi {R_d}^2\xi \quad (2)$$

In these equations, the bending modulus, κ_B, the edge energy, λ, and the effective adhesive contact potential, ξ, are the physical parameters of the lipid bilayer. The radius of the cylinder, R_c, the length of the cylinder, L_c, and the radius of the disk, R_d, are the geometrical parameters of the bilayer. The first term on the right-hand side measures the change in the bending energy to change the curvature of the bilayer, the second term measures the change in the edge energy if breaks in the bilayer must form to allow budding at a constant area, and the third term measures the change in adhesion energy to separate the bilayers. We take that the bilayers are in a stack of multiple bilayers. Thus, the effective adhesive contact potential, ξ, is that of bilayers interacting with each other.

The free energy change to form a spherical bud from a cylindrical bilayer can be negative while the free energy change to form a spherical bud from a flat bilayer is always positive.[16,19] This result can be readily shown by using the characteristic dimensions of a cylindrical bilayer on a nanocellulose fiber, R_c = 20 nm, L_c = 2000 nm and a flat disk R_d = 242 nm, and with $\kappa_B = 8.5 \times 10^{-20}$ J, $\lambda = 1 \times 10^{-11}$ J m^{-1}, and $\xi = -1 \times 10^{-5}$ J m^{-2} for DOPC.[58] The energy to form a bud of radius R_B = 141 nm from the cylindrical bilayer is $\Delta E_{R_B,c} \approx -4754\ k_BT$ and from the flat bilayer is $\Delta E_{R_B,d} \approx 5439\ k_BT$. Here the energy is expressed relative to the thermal energy scale $1\ k_BT = 4.11 \times 10^{-21}$ J. Because of the large and positive free energy change for the formation of buds from flat bilayers relative to the thermal energy scale, the formation of most GUV-sized buds occurs within 1 minute of hydration due to energy released upon hydration.[19] For the PAPYRUS method, in addition to bud formation upon hydration, additional nanoscale buds form and merge up to 30 minutes post-hydration.[19] Merging of the nanoscale buds with each other and with GUV-sized buds results in a higher molar yield and a greater fraction of GUVs with $d \geq$ 10 μm compared to the gentle hydration method. The budding and merging model is consistent with the assembly of GUVs using pure DOPC.

We consider changes to the physical constants of the membrane which could explain the effect of incorporation of PEG2000-DSPE on the yield of GUVs. To explain the observed results, there should be no change in the magnitude of the free energy change for bud formation from cylindrical bilayers whereas the magnitude of the free energy change for bud formation from flat disk-shaped bilayers should be greatly reduced. Keeping the same geometrical parameters, a hypothetical reduction of the magnitude of κ_B by five times to 1.7×10^{-20} J results in $\Delta E_{R_B,c} = 27.5\ k_BT$ and $\Delta E_{R_B,d} = 5023\ k_BT$. Taking the limit of no adhesion between bilayers, $\xi = 0$, $\Delta E_{R_B,c} = -5367\ k_BT$ and $\Delta E_{R_B,d} = 4831\ k_BT$. Taking the limit of no edge

energy, $\lambda = 0$, $\Delta E_{R_B,c} = -5366\ k_BT$ and $\Delta E_{R_B,d} = 1128\ k_BT$. We surmise that, (i) a change in the bending modulus can have a large effect on the free energy change of budding from cylindrical bilayers but has a small effect on the free energy change of budding from flat bilayers, (ii) a change in the adhesive contact potential results in similar changes in the magnitudes of the free energy change of budding from cylindrical bilayers and flat bilayers, and (iii) a change in the edge energy has a small effect on the free energy change of budding from cylindrical bilayers but can have a large effect on the free energy change of budding from flat bilayers.

Since putative changes in the physical parameters of the membrane do not provide a conclusive explanation for our results, we hypothesized that an additional pathway of assembly other than budding and merging may be operational in membranes containing 3 mol% of PEG2000-DSPE.

3.2 Films of DOPC + 3 mol% PEG2000-DSPE form a foam-like mesophase on glass but not on nanocellulose paper

To test our hypothesis, we probed directly by imaging the lipid films using high-resolution confocal microscopy. We show representative orthogonal x–z slices in the upper panels and x–y sum projections in the lower panels of Fig. 2a–d. We enhance the contrast of the x–z slices using histogram equalization to show both bright and dim regions. We show the original non-contrast enhanced images in ESI,† Fig. S3. The other images in Fig. 2 retain their original intensity values.

Similar to previous reports, GUV-sized buds were abundant and close-packed on the surface of nanocellulose paper for the lipid composition consisting of pure DOPC (Fig. 2a).[19] The samples prepared with DOPC + 3 mol% PEG2000-DSPE did not show any apparent differences from the samples consisting of pure DOPC (Fig. 2b). Both samples had buds that appeared as 5–6 size stratified layers above the surface of the paper (Fig. 2a and b). On the glass slide, buds on the lipid film consisting of pure DOPC formed a single layer on the surface and appeared sparse compared to the buds on the surface of nanocellulose paper (Fig. 2c).[19] The sample prepared with DOPC + 3 mol% PEG2000-DSPE on the glass slide however showed a marked difference compared to the other three samples. The lipid film formed a voluminous mesophase that extended up to 130–160 μm from the surface of the glass (Fig. 2d). The mesophase had non-fluorescent polyhedral and spherical regions of the aqueous continuous phase that were bounded by the fluorescent lipid membranes. In appearance, the mesophase was reminiscent of a foam. We thus refer to this mesophase as a "foam-like" mesophase. The foam-like mesophase is composed of lamellar lipid membranes and is fully suspended in an aqueous phase. It is thus not a true two-phase foam, which is a gaseous phase dispersed in a liquid or solid phase.

We highlight key areas in the image using white and red arrows and show x–y slices corresponding to these locations in Fig. 2e–g. The region closest to the glass slide consisted of a few

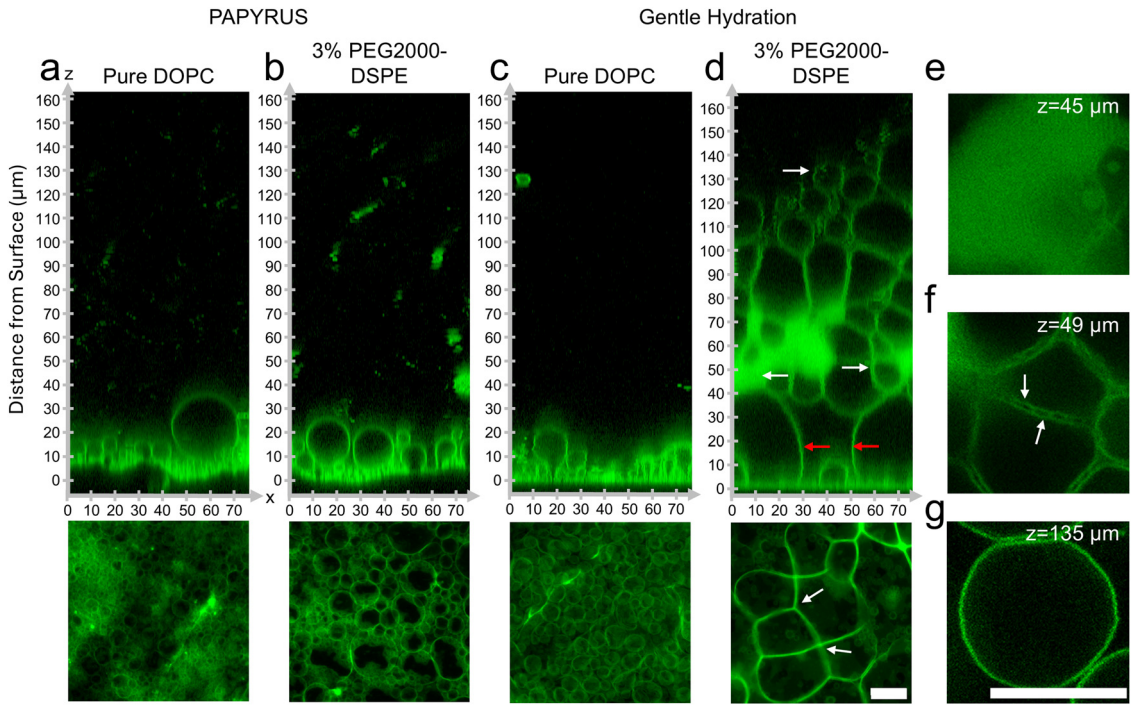

Fig. 2 Configuration of the hydrated lipid films containing pure DOPC and DOPC + 3 mol% PEG2000-DSPE. (a)–(d) Upper panels show orthogonal x–z planes of confocal Z-stacks of the lipid films on the surface. Bottom panels are x–y planes consisting of summed z-projections of the first 18 μm from the surface of the substrate. (a) Pure DOPC on nanocellulose paper. (b) DOPC + 3 mol% PEG2000-DSPE on nanocellulose paper. (c) Pure DOPC on glass. (d) DOPC + 3 mol% PEG2000-DSPE on glass. The red arrows show the lipid septa in the mesophase. (e)–(g) x–y slices from the regions indicated by the white arrows in (d). Scale bars are 15 μm.

spherical buds located between large, connected membrane septa (red arrows in Fig. 2d). The septa met at vertices of 3 to 4 septa (white arrows in Fig. 2d lower panel). Further away from the surface, the mesophase had lipid dense regions, regions of separated septa, and pockets of GUV-like spherical structures. The lipid dense regions appear to have regions of low fluorescence intensities, which we interpret to be regions of continuous phase (Fig. 2e). These regions of low intensity were in a lattice with hexagonal symmetry 1 μm apart (see ESI,† Fig. S4 showing zoomed images and fast Fourier transforms (FFT) of the images). The lipid dense regions appeared connected and continuous with the separated septa. In this region, the septa enclosed the continuous phase forming polyhedral cells (Fig. 2f). Unlike the septa on the surface, the septa in this middle region show two clearly distinguishable membranes that appear to touch at 2 ± 0.6 μm intervals (white arrows in Fig. 2f). Further away from the surface and in regions within the mesophase, pockets of spherical GUV-like objects were evident (Fig. 2g).

Since the mesophase appears to correlate with the ultrahigh yields of GUVs, we probed the dynamics of the formation of the mesophase. We captured confocal Z-stacks at 7 minutes, 30 minutes, and 60 minutes (Fig. 3a). See ESI,† Fig. S5 for original non-contrast enhanced images. Remarkably, the mesophase was already present at 7 minutes after hydration and remains relatively unchanged at 30 minutes and 60 minutes. The GUV yield obtained by harvesting at 10 minutes was 52 ± 1% which was statistically indistinguishable from the sample harvested at 60 minutes (p = 0.118). We show a histogram of the distribution of GUV diameters in ESI,† Fig. S6. We conclude that the GUVs originate from this foam-like mesophase and can, in principle, be obtained within 10 minutes. This mode of obtaining GUVs from a volume-spanning lamellar mesophase with the inclusion of the 3 mol% PEG2000-DSPE is distinct from surface-attached budding and merging of pure DOPC bilayers, explaining why the budding and merging model could not describe the measured yields. The rapid formation of the mesophase is consistent with the expectation that the energy released upon hydration drives the dynamics of the lipid films on flat surfaces.[19] Evidently, the enmeshed nanocellulose fibers of nanocellulose paper inhibits the formation of the foam-like lipid mesophase.

To further understand this alternative GUV formation pathway, we characterize the surface configuration of the films, the yield, and the size distributions of the harvested population of GUVs, (i) with various mol% of PEG2000-DSPE, (ii) with lipids that have partial molecular similarity to PEG2000-DSPE, (iii) with different lipid compositions, and (iv) with flat surfaces of different types.

3.3 The configuration of the lipid film on the surfaces and the molar yields are affected by the mol% PEG2000-DSPE

We assembled GUVs using the gentle hydration method with mixtures consisting of DOPC and 0.1, 1, 5, and 10 mol% of PEG2000-DSPE. Changes in the mol% of PEG2000-DSPE affects the physical properties of the membranes. Increasing the mol% of the PEG2000-DPSE increases the surface charge density of the membrane and causes the PEG2000 chain to transition from a gas of globular mushrooms to extended brushes.[35,40] This transition is gradual, and occurs when a fluid phase membrane contains 3–5 mol% of PEG2000-DSPE. At these concentrations, the distance between the PEG2000-DSPE molecules

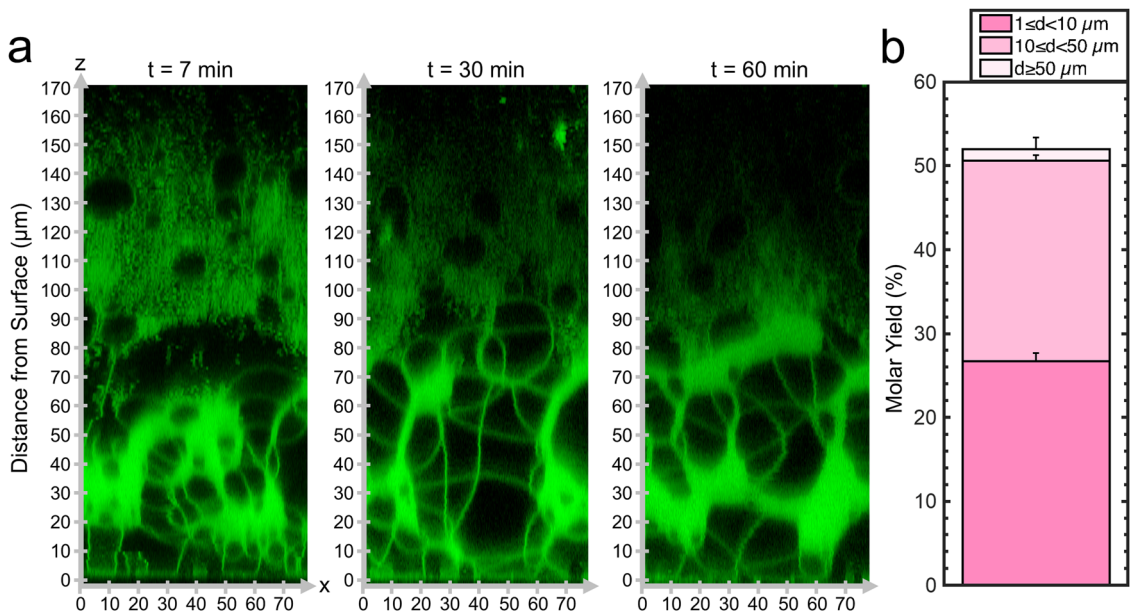

Fig. 3 Dynamics of the lipid-dense mesophase formed from DOPC + 3 mol% PEG2000-DSPE. (a) Orthogonal x–z planes of confocal Z-stacks of the assembled mesophase over time. (b) Molar yield of GUVs harvested after 10 minutes of incubation. The stacks show the percentage of the molar yield that is comprised of the size classifications as listed in the legend. The data is an average of n = 3 independent repeats. The error bars are one standard deviation from the mean.

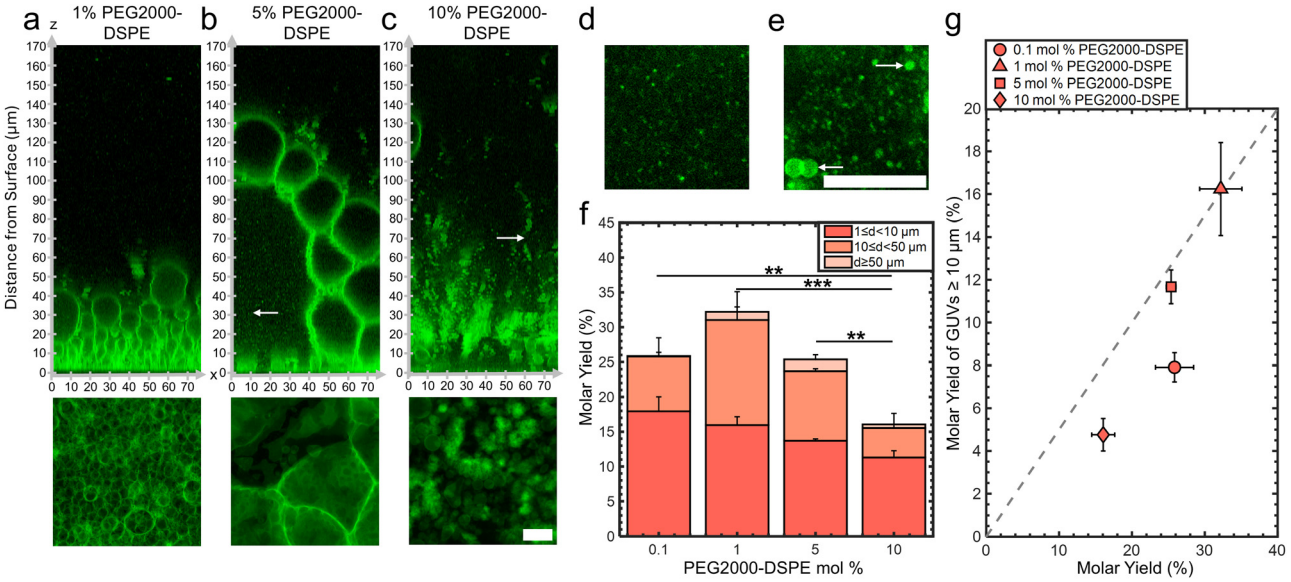

Fig. 4 Effect of the mol% of PEG2000-DSPE on the configuration of the film and molar yields. (a)–(c) Upper panels show orthogonal x–z planes of confocal Z-stacks of the lipid films on the surface. Bottom panels are x–y planes consisting of summed z-projections of the first 18 μm from the surface of the substrate. (a) DOPC + 1 mol% PEG2000-DSPE. (b) DOPC + 5 mol% PEG2000-DSPE. (c) DOPC + 10 mol% PEG2000-DSPE. Example of small micelle-like structures from the region shown by the white arrow in (b) and (c). (d) 5 mol% PEG2000-DSPE. (e) 10 mol% PEG2000-DSPE. The large bright objects are GUVs and MLVs (white arrows). (f) Molar yields of GUVs with increasing mol% of PEG2000-DSPE. The stacks show the percentage of the molar yield that is comprised of the size classifications as listed in the legend. Each bar is an average of n = 3 independent repeats. Statistical significance was determined using a balanced one-way ANOVA and Tukey's HSD *post hoc* tests. (g) Scatter plot showing the molar yield from GUVs ≥ 10 μm in diameter *versus* the total molar yield. Each data point is the average of n = 3 independent repeats. The grey dashed line indicates where half the lipid molecules are in GUVs with diameters ≥ 10 μm. Scale bars are 15 μm.

falls below twice the Flory radius, R_F = 3.66 nm of PEG2000.[35,40] Additionally, high mol% of PEG2000-DSPE in membranes favors the formation of micellar phases.[38,40]

Confocal images show that the lipid film after 1 hour demonstrated configurations that depended on the mol% of PEG2000-DSPE (Fig. 4a–c). See ESI,† Fig. S7 for the original non-contrast enhanced images. In mixtures containing 0.1 and 1 mol% PEG2000-DSPE, GUV-sized buds were present on the surface. There was no noticeable difference between the configuration of buds for pure DOPC and the DOPC + 0.1 mol% PEG2000-DSPE mixture (image not shown). In contrast, the DOPC + 1 mol% PEG2000-DSPE mixture had 5–6 stacked layers of buds, similar to the configuration of the buds on the surface of nanocellulose paper (compare Fig. 4a with Fig. 2a and b). For the DOPC + 5 mol% PEG2000-DSPE mixture, a volume-spanning foam-like mesophase that was qualitatively similar to the DOPC + 3 mol% of PEG2000-DSPE mixture was present. However, this mesophase had a noticeably lower lipid density than the mesophase that formed with the DOPC + 3 mol% PEG2000-DSPE mixture. The lower lipid density is apparent by the large fraction of continuous phase between the septa and the lack of lipid dense regions. For the DOPC + 10 mol% PEG2000-DSPE mixture, the foam-like mesophase was no longer evident. Instead, structures that appeared to be clusters of detached GUVs, the majority that have diameters <10 μm, appeared to form. Very few buds were attached to the surface. Both the 5 mol% and 10 mol% PEG2000-DSPE had regions with small bright speckles that diffused freely (white arrows in Fig. 4b and c, x–y images in Fig. 4d and e). These bright speckles were not present in mixtures containing 3 mol% or lower of PEG2000-DSPE. These speckles are consistent with micelles that are known to form in mixtures with high mol% of PEG2000-DSPE.[38,40]

Fig. 4f shows a plot of the molar yields obtained using the lipid mixtures. We show representative images of the harvested objects and histograms of the size distributions in ESI,† Fig. S8 and S9. For 0.1,1, 5, and 10 mol% of PEG2000-DSPE, the molar yield was 26 ± 3%, 32 ± 3%, 25 ± 1%, and 16 ± 2%, respectively. In addition to the DOPC + 3 mol% PEG2000-DSPE lipid mixture, only the DOPC + 1 mol% PEG2000-DSPE lipid mixture showed a yield significantly different from pure DOPC ($p = 7.76 \times 10^{-4}$). Furthermore, this yield was statistically indistinguishable from the yield of GUVs obtained using the PAPYRUS method (p = 0.348). For lipid mixtures with 0.1, 1, 5, and 10 mol% of PEG2000-DSPE, the fraction of GUVs with $d \geq 10$ μm was 31%, 50%, 46%, and 30%, respectively (Fig. 4g). Thus, the DOPC + 1 mol% PEG2000-DSPE and DOPC + 5 mol% PEG2000-DSPE lipid mixtures had a higher fraction of GUVs with $d \geq 10$ μm compared to pure DOPC. The DOPC + 0.1 mol% PEG2000-DSPE, and DOPC + 10 mol% PEG2000-DSPE lipid mixtures had lower fraction of GUVs with $d \geq 10$ μm compared to pure DOPC. All these mixtures had a lower fraction of GUVs with $d \geq 10$ μm compared to pure DOPC obtained using the PAPYRUS method and compared to DOPC + 3 mol% PEG2000-DSPE obtained using the PAPYRUS and the gentle hydration methods.

To surmise, only the mixtures containing 1 and 3 mol% of PEG2000-DSPE resulted in yields significantly different from pure DOPC, and only the mixture containing 3 mol% PEG2000-DSPE had ultrahigh yields. Consistent with their similar surface configuration of a close-packed layer of size-stratified buds, the lipid mixture containing 1 mol% of PEG2000-DSPE had similar yields to the PAPYRUS method despite the flat geometry of the surface. All the other compositions, despite showing similar yields to pure DOPC, had different configurations of hydrated lipid on the surfaces. The DOPC + 0.1 mol% PEG2000-DSPE lipid mixture showed similar configuration of a single sparse layer of buds to pure DOPC, the DOPC + 5 mol% PEG2000-DSPE lipid mixture had a lipid-poor foam-like mesophase and micelles, while the DOPC + 10 mol% PEG2000-DSPE lipid mixture had clusters of detached GUVs and micelles. These results show that similar yields of GUVs could arise from different configurations of the hydrated lipid on surfaces.

3.4 Long-range electrostatic and short-range steric interactions are both needed for the formation of the lipid-dense foam-like mesophase and for obtaining ultrahigh yields

We investigated the molecular mechanism for the formation of the foam-like mesophase by using lipids with partial molecular similarity to PEG2000-DPSE. We prepared lipid films composed of DOPC with 3 mol% DSPE, 3 mol% PEG2000-DSG, or 3 mol% DSPG. Fig. 5a shows the structures of the lipids relative to PEG2000-DSPE. DSPE is the lipid portion of PEG2000-DSPE. PEG2000-DSG has a poly(ethylene glycol) chain similar to PEG2000-DSPE but does not have a negatively charged phosphate group. DSPG has a negatively charged phosphate group similar to the negatively charged phosphate group of PEG2000-DSPE but does not have a poly(ethylene glycol) chain. Confocal images show that the films form surface-attached buds for all three lipid mixtures. There is no foam-like mesophase (Fig. 5b). See ESI,† Fig. S10 for the original non-contrast enhanced images. Furthermore, we find that none of the lipid mixtures resulted in GUV yields significantly different from pure DOPC, albeit the distributions in sizes were different (Fig. 6a). We find that the addition of 3 mol% of DSPE, PEG2000-DSG, and DSPG resulted in a yield of 16 ± 0.5%, 17 ± 3%, and 26 ± 2% respectively. The fraction of GUVs with $d \geq 10$ μm for DSPE, DSPG, and PEG2000-DSG was 25%, 48%, and 35% respectively (Fig. 6b).

Since PEG2000-DSG had no effect on the yield of GUVs, we reasoned that the formation of the foam-like mesophase and the increase in yield requires the charge group in addition to the poly(ethylene glycol) chain. The range of the electrostatic interaction is highly sensitive to the ionic strength of the solution. The Debye screening length provides an estimate of the range of electrostatic interaction.[58] At the Debye length, the electrostatic potential decays by $1/e$. To test the relative importance of the range of the electrostatic interaction for forming the foam-like mesophase, we hydrated films of DOPC + 3 mol% PEG2000-DSPE in 100 mM sucrose + 1 mM NaCl and in 100 mM sucrose + phosphate buffered saline (PBS) (PBS composition: 137 mM NaCl, 2.7 mM KCl, 8 mM Na_2HPO_4, and 2 mM KH_2PO_4). The Debye screening lengths are 170 nm, 9.6 nm, and 0.75 nm in 100 mM sucrose, 100 mM sucrose + 1 mM of NaCl, and 100 mM sucrose + PBS, respectively. Thus, in these solutions, the screening lengths are ∼37×, 2×, and 0.2× the Flory radius of PEG2000-DSPE. The yield of GUVs dropped to 23 ± 2% in the solution with 1 mM NaCl (Fig. 6c). In PBS, the yield of GUVs was 0.8 ± 0.2%.[15] Upon the inclusion of salt, the fraction of molar yield from GUVs with $d \geq 10$ μm reduced to 21% in the solution containing 1 mM NaCl and to 4% in PBS (Fig. 6d). See ESI,† Fig. S11 and S12 for representative images of the harvested objects and histograms of the sizes.

We conclude that the formation of the foam-like mesophase is unique to PEG2000-DSPE and requires both the short-range steric repulsion of the poly(ethylene glycol) chain and the long-range repulsion of the phosphate group. In molecularly similar

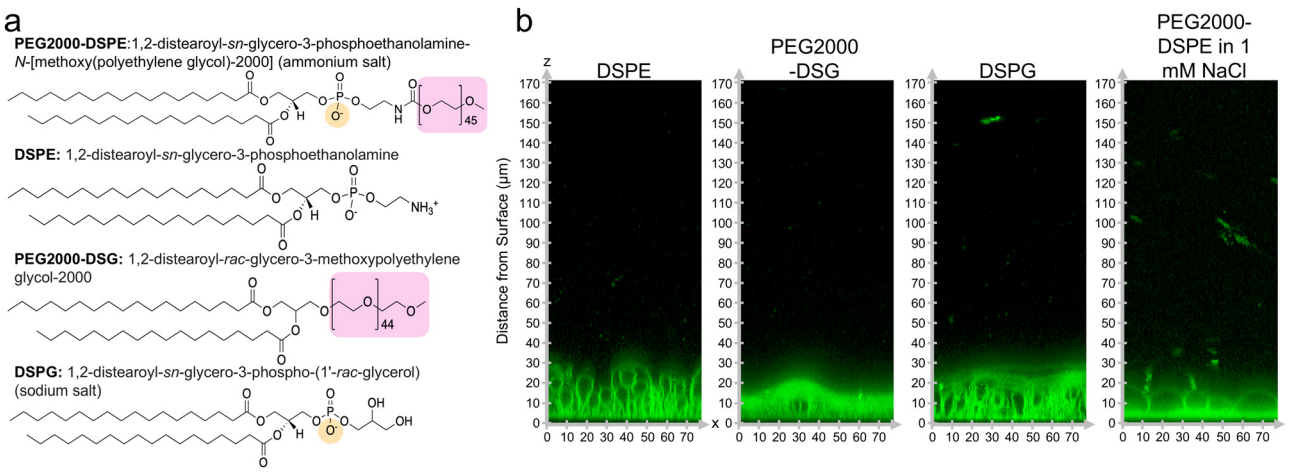

Fig. 5 Chemical structures of lipids and configuration of the films on the surface. (a) Chemical structures of lipids used. The PEG chain is highlighted in pink and the negative charge is highlighted in yellow. (b) Orthogonal x–z planes of confocal Z-stacks of the lipid films on the surface after 1 hour of hydration.

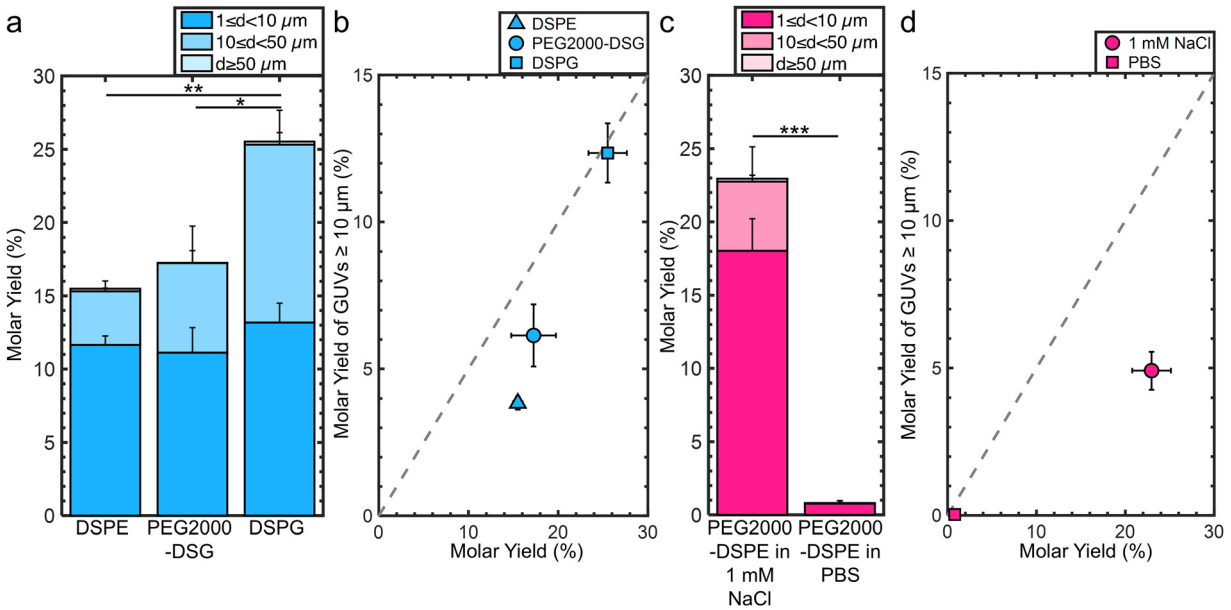

Fig. 6 Molar yields of GUVs assembled with lipids with partial molecular similarity to PEG2000-DSPE. (a) Stacked bar plots showing molar yields from the gentle hydration method with DOPC + 3 mol% DSPE, DOPC + 3 mol% PEG2000-DSG, and DOPC + 3 mol% DSPG. (b) Scatter plot showing the molar yield from GUVs ≥ 10 μm in diameter *versus* the total molar yield for DOPC + 3 mol DSPE, DOPC + 3 mol PEG2000-DSG and DOPC + 3 mol dspg. (c) Stacked bar plots showing molar yields from the gentle hydration method with DOPC + 3 mol% PEG2000-DSPE in 100 mm sucrose + 1 mm NaCl and 100 mm sucrose + PBS. (d) Scatter plot showing the molar yield from GUVs ≥ 10 μm in diameter *versus* the total molar yield. The grey dashed line indicates where half the lipid molecules are in GUVs with diameters ≥ 10 μm. The stacks show the percentage of the molar yield that is comprised of the size classifications as listed in the legend. Each data point is the average of n = 3 independent repeats. The error bars are one standard deviation from the mean. Statistical significance was determined using a balanced one-way anova and tukey's hsd *post hoc* tests when comparing multiple means or a student's t-test when comparing two means. *: $p < 0.05$, **: $p < 0.01$, ***: $p < 0.001$, n.s.: not significant.

lipids lacking one of these interactions, or when the range of electrostatic repulsion is reduced by screening in salty solutions, the mesophase does not form.

3.5 Addition of PEG2000-DSPE increases yields of GUVs of complex lipid mixtures, on stainless steel substrates, and in the electroformation method on ITO slides

We determine the generality of the strategy of incorporating 3 mol% PEG2000-DSPE to increase the molar yield and fraction of large GUVs. We conducted experiments that varied the lipid composition, the identity of flat substrate, and employed the electroformation method on ITO slides.

For the experiments testing lipid composition, we use a ternary mixture consisting of the unsaturated lipid DOPC, the saturated lipid DPPC, and cholesterol as our model lipid composition. This lipid composition is a canonical mixture used to study lateral phase separation and membrane organization.[59,60] Without PEG2000-DSPE, the molar yield was 21 ± 1%. 25% of the molar yield was from GUVs with $d \geq$ 10 μm. Incorporation of 3 mol% PEG2000-DSPE results in a 1.7× increase in the molar yield to 36 ± 3% and a 1.4× increase of the molar yield from GUVs with $d \geq$ 10 μm (Fig. 7a and b). We show representative images and histograms of the sizes in ESI,† Fig. S13.

For the experiments testing the identity of flat substrate, we use stainless steel sheets because it is a durable material used to fabricate sterilizable tools for biomedical applications.[61] Without PEG2000-DSPE, the molar yield was 19 ± 3%. 19% of the molar yield was from GUVs with $d \geq$ 10 μm. Incorporation of 3 mol% PEG2000-DSPE results in a 2.1× increase in the molar yield to 40 ± 3% and a 1.6× increase in the molar yield of GUVs with $d \geq$ 10 μm (Fig. 7c and d). We show representative images and histograms of the sizes in ESI,† Fig. S14.

For the electroformation method, we find without PEG2000-DSPE, the molar yield was 17% (ESI,† Fig. S15a).[16,19] 37% of the molar yield was from GUVs with $d \geq$ 10 μm. Incorporation of 3 mol% PEG2000-DSPE results in a 2× increase in the molar yield to 34% and 1.3× of the increase of the molar yield was from GUVs with $d \geq$ 10 μm (ESI,† Fig. S15b). We show representative images and histograms of the sizes in ESI,† Fig. S16.

In all these conditions, the inclusion of 3 mol% PEG2000-DSPE results in an increase in molar yield of GUVs and an increase in the fraction of large GUVs. Thus, we conclude that adding PEG2000-DSPE to lipid mixtures could be a general strategy to increase the yields and fraction of large GUVs obtained using the gentle hydration method on planar surfaces and electroformation on ITO slides in low salt solutions.

3.6 Shear induced fragmentation of the foam-like mesophase contributes to the formation of ultrahigh yields of GUVs in mixtures containing 3 mol% PEG2000-DSPE

We show in Fig. 8 schematics of the proposed mechanism of the assembly of GUVs in the presence of PEG2000-DSPE.

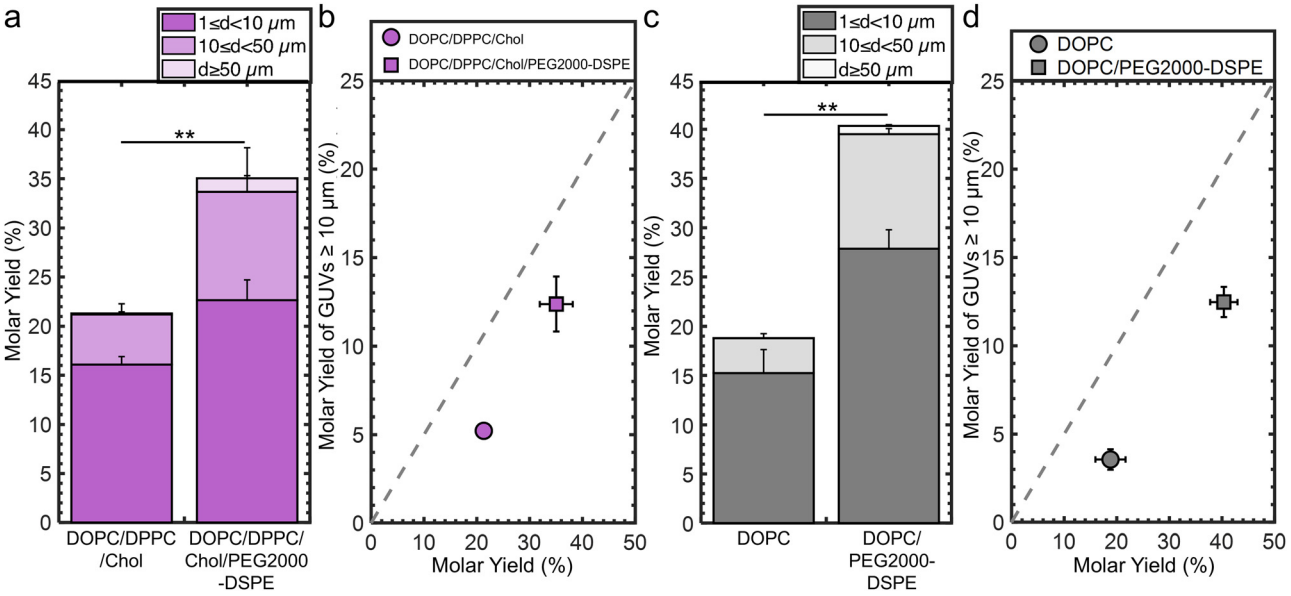

Fig. 7 Generality of increasing yields by adding 3 mol% of PEG2000-DSPE. (a) Molar yield of GUVs composed of DOPC/DPPC/cholesterol and DOPC/DPPC/cholesterol + 3 mol% PEG2000-DSPE. (b) Scatter plot showing the molar yield from GUVs ≥ 10 μm in diameter *versus* the total molar yield for the samples in (a). (c) Molar yield of GUVs composed of pure DOPC and DOPC + 3 mol% PEG2000-DSPE obtained using the gentle hydration method on stainless steel sheets. (d) Scatter plot showing the molar yield from GUVs ≥ 10 μm in diameter *versus* the total molar yield for the samples in (c). The stacks show the percentage of the molar yield that is comprised of the size classifications as listed in the legend. Each bar is an average of $n = 3$ independent repeats. Each data point is the average of $n = 3$ independent repeats. The error bars are one standard deviation from the mean. The grey dashed line indicates where half the lipid molecules are in GUVs with diameters ≥ 10 μm. Statistical significance was determined using a student's *t*-test. *: $p < 0.05$, **: $p < 0.01$, ***: $p < 0.001$, n.s.: not significant.

From 0 to 1 mol% PEG2000-DSPE, GUV-sized buds assemble through budding and merging on the surface (Fig. 8a and b). We propose that concentrations of 0.1 mol% and lower do not change the physical parameters of the bilayer enough to result in statistically significant changes in the yield compared to using pure DOPC (Fig. 8a). At 1 mol% of PEG2000-DSPE, the increase in buds obtained *via* budding and merging on the glass surface could be due to changes in the membrane physical parameters such as a decrease in the membrane adhesion potential, edge energy, or bending rigidity (Fig. 8b).

At 3 mol% PEG2000-DSPE, we propose that the repulsive forces contributed by both the long-ranged electrostatic interactions and short-ranged steric interactions causes the rapid expansion of the film to form a lipid-dense foam-like mesophase (Fig. 8c). GUVs assemble due to shear-induced fragmentation and closure of the membranes in the mesophase when the pipette is used for harvesting. Two lines of evidence support this proposed mechanism. (1) The median size of GUVs, 3.9 ± 0.1 μm, is smaller than the median size of the polyhedral cells in the mesophase, 25 ± 10 μm. This observation suggests that the large structures in the mesophase break up. (2) The mesophase is present within 7 minutes and harvesting using the pipette at 10 minutes shows a similar yield of GUVs to harvesting at 60 minutes. This observation suggests that self-assembly of the mesophase over the duration of 1 hour is not needed to obtain the GUVs. The GUVs are obtained upon application of fluid shear during harvesting, be it at 10 minutes or 60 minutes.

Although similar shear-induced fragmentation is expected to occur at 5 mol% of PEG2000-DSPE (Fig. 8d), micellization reduces the density of lamellar membranes. At 10 mol% of PEG2000-DSPE, the mesophase appears to lose integrity (Fig. 8e). We propose that at this high mol% of PEG2000-DSPE, the lipids are mainly in micelles and only small clusters of GUVs remain on the surface. The micellization at these higher PEG2000-DSPE mol% results in the reduction in GUV yields.

With the conditions of assembly that we employed, having a substrate with flat geometry is essential for the formation of the foam-like mesophase. The cylindrical geometry and the entangled fibers of nanocellulose paper appear to prevent the formation of the mesophase. Instead, buds evolve on the surface due to budding and merging even when 3 mol% or PEG2000-DSPE is present in the membrane.

4 Summary and outlook

This work shows that incorporation of PEG2000-DSPE results in complex but measurable effects on both the yield of GUVs and configuration of the lipid film on the surface. The complex effects that we find belie simplistic correlation to changes in a single physical parameter of the membrane, such as an expected increase in intermembrane repulsion,[35–37] upon incorporation of PEG2000-DSPE. At 1 mol% of PEG2000-DSPE, there are size-stratified layers of surface-attached GUV-sized buds on the surface, while at 3 mol% PEG2000-DSPE,

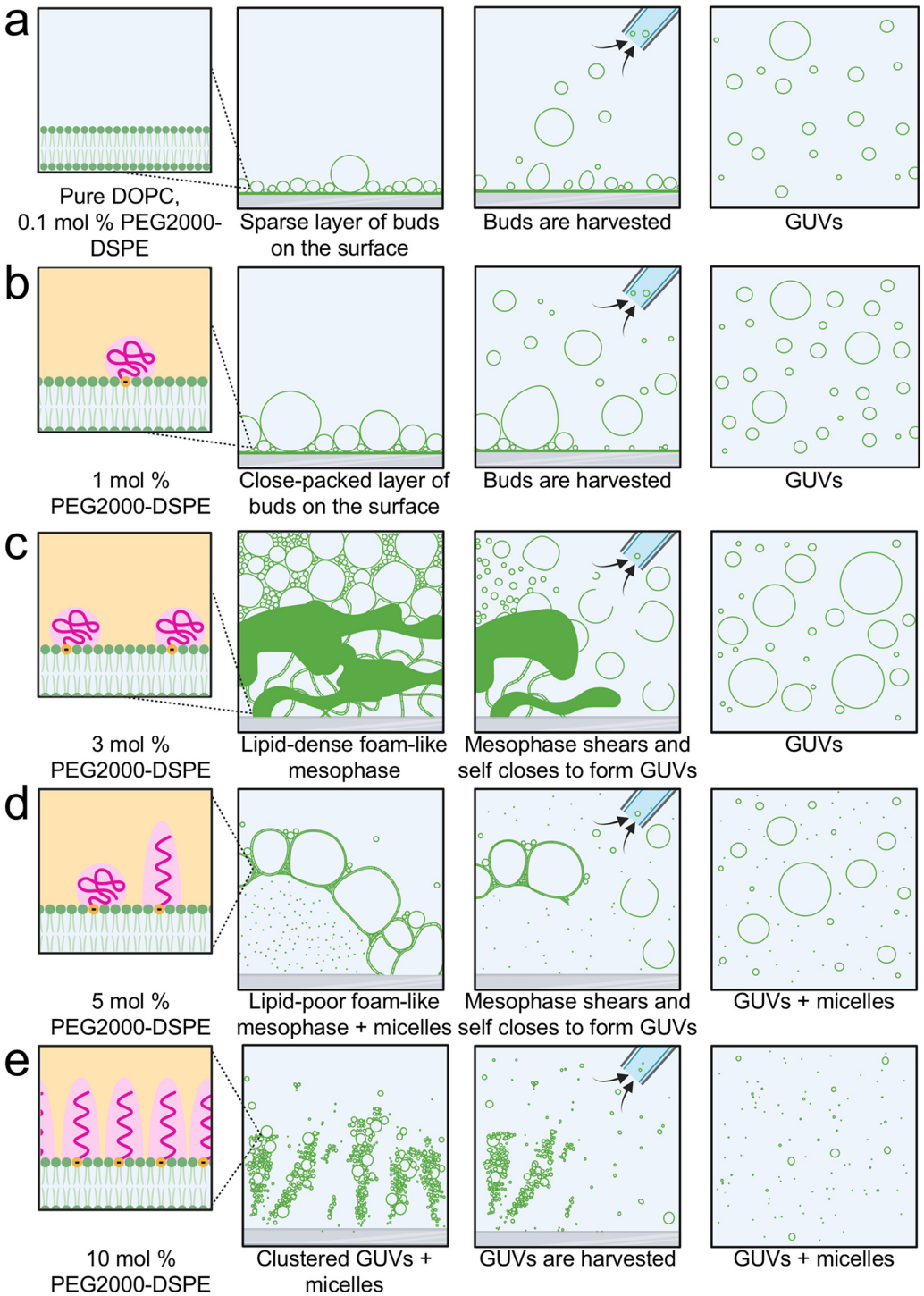

Fig. 8 Schematic of pathways of assembly of GUVs in lipid mixtures containing varying mol% of PEG2000-DPSE. (a) Pure DOPC and DOPC + 0.1 mol% PEG2000-DSPE. (b) DOPC + 1 mol% PEG2000-DSPE. (c) DOPC + 3 mol% PEG2000-DSPE. (d) DOPC + 5 mol% PEG2000-DSPE. (e) DOPC + 10 mol% PEG2000-DSPE.

a foam-like lipid dense mesophase forms that is broken up during harvesting. Fragmentation of this lipid dense mesophase is a pathway of assembly that can result in ultrahigh yields of GUVs. At 5 mol% of PEG2000-DSPE, the mesophase becomes lipid poor before appearing to disintegrate at 10 mol% of PEG2000-DSPE.

Incorporating 3 mol% of PEG2000-DSPE in a phase separating mix and on stainless steel substrates is effective in doubling the yields of GUVs compared to mixtures without PEG2000-DSPE. This effect appears to be unique to PEG2000-DSPE and does not occur in lipids with partial molecular similarity such as those that only have a charged phosphate headgroup or only

a PEG2000 chain. Furthermore, when the range of the electrostatic interaction of the charged phosphate headgroup on PEG2000-DSPE is screened, the yield of GUVs falls. The yield of GUVs becomes negligible in solutions of physiological ionic strength.

From a mechanistic perspective, this work reports the discovery of an alternate pathway for forming GUVs *via* mesophase break up of membranes containing 3 and 5 mol% PEG2000-DSPE. This pathway is distinct from budding and merging on surfaces.[19] Thus, two different pathways that depend on the membrane composition and the geometry of the surface can result in the assembly of GUVs from thin lipid films.

Looking forward, we anticipate other factors such as the surface concentration of lipid and the composition of the membrane could favor the formation of GUVs *via* one pathway over the other. The framework that couples quantitative measurements of yield with direct high-resolution visualization of the lipid film that we use here could be useful for understanding these other conditions. Furthermore, PEG2000-DSPE in the range of 1 to 3 mol% is used widely in clinical applications[27,28] and surfaces such as stainless steel are used in bioreactor chambers.[61] Our results show that in addition to conferring properties such as ''stealth'' capabilities and increased circulation lifetime, addition of 1 to 3 mol% of PEG2000-DSPE into lipid mixtures provides a route to obtaining high and ultrahigh yields of GUVs *via* the gentle hydration method using myriad planar substrates.

Author contributions

A. B. S. conceived and directed the study. A. C. performed experiments and analyzed the data. A. B. S. and A. C. interpreted the data. A. B. S. proposed the shear-induced fragmentation mechanism. A. C. prepared the figures. A. B. S. and A. C. wrote the manuscript. All authors have given approval to the final version of the manuscript.

Data availability

The data supporting this article have been included in the manuscript.

Conflicts of interest

There are no conflicts to declare.

Acknowledgements

This work was funded by the National Science Foundation through NSF CAREER DMR-1848573. The data in this work was collected, in part, with a confocal microscope acquired through the National Science Foundation MRI Award Number DMR-1625733. The schematic in Fig. 8 and the table of contents graphic were created in BioRender. Cooper, A. (2024) **https://BioRender.com/r17o385**, **https://BioRender.com/o46b605**.

References

1 K. S. Nair and H. Bajaj, *Adv. Colloid Interface Sci.*, 2023, **318**, 102935.
2 M. J. York-Duran, M. Godoy-Gallardo, C. Labay, A. J. Urquhart, T. L. Andresen and L. Hosta-Rigau, *Colloids Surf., B*, 2017, **152**, 199–213.
3 C. Has and P. Sunthar, *J. Liposome Res.*, 2020, **30**, 336–365.
4 M. Imai, Y. Sakuma, M. Kurisu and P. Walde, *Soft Matter*, 2022, **18**, 4823–4849.
5 R. W. Jaggers and S. A. F. Bon, *Soft Matter*, 2018, **14**, 6949–6960.
6 H. Wan, G. Jeon, G. M. Grason and M. M. Santore, *Soft Matter*, 2024, **20**, 6984–6994.
7 L. Parolini, B. M. Mognetti, J. Kotar, E. Eiser, P. Cicuta and L. Di Michele, *Nat. Commun.*, 2015, **6**, 5948.
8 R. Cao, D. Kumar and A. D. Dinsmore, *Langmuir*, 2021, **37**, 1714–1724.
9 G. Chen, R. Levin, S. Landau, M. Kaduri, O. Adir, I. Ianovici, N. Krinsky, O. Doppelt-Flikshtain, J. Shklover, J. Shainsky-Roitman, S. Levenberg and A. Schroeder, *Proc. Natl. Acad. Sci. U. S. A.*, 2022, **119**, 1–9.
10 O. Thaden, N. Schneider, T. Walther, E. Spiller, A. Taoum, K. Göpfrich and D. Duarte Campos, *ACS Synth. Biol.*, 2024, **13**, 2436–2446.
11 J. E. Hernandez Bücher, O. Staufer, L. Ostertag, U. Mersdorf, I. Platzman and J. P. Spatz, *Biomaterials*, 2022, **285**, 121522.
12 L. Casas-Ferrer, A. Brisson, G. Massiera and L. Casanellas, *Soft Matter*, 2021, **17**, 5061–5072.
13 Q. Li, S. Li, X. Zhang, W. Xu and X. Han, *Nat. Commun.*, 2020, **11**, 232.
14 F. C. Tsai and G. H. Koenderink, *Soft Matter*, 2015, **11**, 8834–8847.
15 A. Cooper, V. Girish and A. B. Subramaniam, *Langmuir*, 2023, **39**, 5579–5590.
16 J. Pazzi and A. B. Subramaniam, *ACS Appl. Mater. Interfaces*, 2020, **12**, 56549–56561.
17 A. D. Bangham, M. M. Standish and J. C. Watkins, *J. Mol. Biol.*, 1965, **13**, 238–252.
18 J. P. Reeves and R. M. Dowben, *J. Cell. Physiol.*, 1969, **73**, 49–60.
19 J. Pazzi and A. B. Subramaniam, *J. Colloid Interface Sci.*, 2024, **661**, 1033–1045.
20 K. I. Akashi, H. Miyata, H. Itoh and K. Kinosita, *Biophys. J.*, 1996, **71**(6), 3242–3250.
21 B. Robinson, T. Steinkühler and J. Dimova, *J. Visualized Exp.*, 2017, 56034.
22 H. M. J. Weakly, K. J. Wilson, G. J. Goetz, E. L. Pruitt, A. Li, L. Xu and S. L. Keller, *Biophys. J.*, 2024, **123**, 3452–3462.
23 K. Maruyama, T. Yuda, A. Okamoto, S. Kojima, A. Suginaka and M. Iwatsuru, *Biochim. Biophys. Acta, Lipids Lipid Metab.*, 1992, **1128**, 44–49.
24 A. Mori, A. L. Klibanov, V. P. Torchilin and L. Huang, *FEBS Lett.*, 1991, **284**, 263–266.
25 D. Needham, K. Hristova, T. J. Mcintosh, M. Dewhirst, N. Wu and D. D. Lasic, *J. Liposome Res.*, 1992, **2**, 411–430.

26 N. V. Efremova, B. Bondurant, D. F. O'Brien and D. E. Leckband, *Biochemistry*, 2000, **39**, 3441–3451.
27 A. Higuchi, T.-C. Sung, T. Wang, Q.-D. Ling, S. S. Kumar, S.-T. Hsu and A. Umezawa, *Polym. Rev.*, 2022, **63**, 394–436.
28 L. M. Ickenstein and P. Garidel, *Expert Opin. Drug Delivery*, 2019, **16**, 1205–1226.
29 O. Staufer, S. Antona, D. Zhang, J. Csatári, M. Schröter, J. W. Janiesch, S. Fabritz, I. Berger, I. Platzman and J. P. Spatz, *Biomaterials*, 2021, **264**, 120203.
30 Ö. Duhan Toparlak, J. Zasso, S. Bridi, M. Dalla Serra, P. Macchi, L. Conti, M.-L. Baudet and S. S. Mansy, *Sci. Adv.*, 2020, **6**, 4920–4938.
31 Y.-Y. Hsu, S. J. Chen, J. Bernal-Chanchavac, B. Sharma, H. Moghimianavval, N. Stephanopoulos and A. P. Liu, *Chem. Commun.*, 2023, **59**, 8806–8809.
32 D. Blanken, P. Van Nies and C. Danelon, *Phys. Biol.*, 2019, **16**, 045002.
33 J. Ventura-Cobos, E. Climent, R. Martínez-Máñez and A. Llopis-Lorente, *Nano Lett.*, 2024, **24**, 14050–14057.
34 A. K. Kenworthy, S. A. Simon and T. J. Mcintosh, *Biophys. J.*, 1995, **68**, 1903–1920.
35 A. K. Kenworthy, K. Hristova, D. Needham and T. J. McIntosh, *Biophys. J.*, 1995, **68**, 1921–1936.
36 T. L. Kuhl, D. E. Leckband, D. D. Lasic and J. N. Israelachvili, *Biophys. J.*, 1994, **66**, 1479–1488.
37 D. Needham, T. J. Mclatosh and D. D. Lasic, *Biochim. Biophys. Acta*, 1992, **1108**, 40–48.
38 K. Hristova and D. Needham, *Macromolecules*, 1995, **28**, 991–1002.
39 S. Belsito, R. Bartucci, G. Montesano, D. Marsh and L. Sportelli, *Biophys. J.*, 2000, **78**, 1420–1430.
40 D. Marsh, R. Bartucci and L. Sportelli, *Biochim. Biophys. Acta, Biomembr.*, 2003, **1615**, 33–59.
41 K. Hristova and D. Needham, *J. Colloid Interface Sci.*, 1994, **168**, 302–314.
42 D. Marsh, *Biophys. J.*, 2001, **81**, 2154–2162.
43 D. D. Lasic, R. Joannic, B. C. Keller, P. M. Frederik and L. Auvray, *Adv. Colloid Interface Sci.*, 2001, 337–349.
44 A. Mahendra, H. P. James and S. Jadhav, *Chem. Phys. Lipids*, 2019, **218**, 47–56.
45 I. Bivas, V. Vitkova, M. D. Mitov, M. Winterhalter, R. G. Alargova, P. Méléard and P. Bothorel, *Giant Vesicles: Perspectives in Supramolecular Chemistry*, 2000.
46 M. Silvander, M. Johnsson and K. Edwards, *Chem. Phys. Lipids*, 1998, **97**, 15–26.
47 K. Hashizaki, H. Taguchi, C. Itoh, H. Sakai, M. Abe, Y. Saito and N. Ogawa, *Chem. Pharm. Bull.*, 2003, **51**, 815–820.
48 H. Lee and R. G. Larson, *Biomacromolecules*, 2016, **17**, 1757–1765.
49 R. Bartucci, M. Pantusa, D. Marsh and L. Sportelli, *Biochim. Biophys. Acta, Biomembr.*, 2002, **1564**, 237–242.
50 E. C. Giakoumatos, L. Gascoigne, B. Gumí-Audenis, Á. G. García, R. Tuinier and I. K. Voets, *Soft Matter*, 2022, **18**, 7569–7578.
51 M. Stepniewski, M. Pasenkiewicz-Gierula, T. R. Og, R. Danne, A. Orlowski, M. Karttunen, A. Urtti, M. Yliperttula, E. Vuorimaa and A. Bunker, *Langmuir*, 2011, **27**, 7788–7798.
52 K. Shohda, K. Takahashi and A. Suyama, *Biochem. Biophys. Rep.*, 2015, **3**, 76–82.
53 Y. Yamashita, M. Oka, T. Tanaka and M. Yamazaki, *Biochim. Biophys. Acta, Biomembr.*, 2002, **1561**, 129–134.
54 M. D. Collins and S. E. Gordon, *J. Visualized Exp.*, 2013, **76**, e50227.
55 C. Herold, G. Chwastek, P. Schwille and E. P. Petrov, *Langmuir*, 2012, **28**, 5518–5521.
56 V. Girish, J. Pazzi, A. Li and A. B. Subramaniam, *Langmuir*, 2019, **35**, 9264–9273.
57 J. Schindelin, I. Arganda-Carreras, E. Frise, V. Kaynig, M. Longair, T. Pietzsch, S. Preibisch, C. Rueden, S. Saalfeld, B. Schmid, J. Y. Tinevez, D. J. White, V. Hartenstein, K. Eliceiri, P. Tomancak and A. Cardona, *Nat. Methods*, 2012, **9**, 676–682.
58 J. N. Israelachvili, *Intermolecular and Surface Forces*, Academic Press, Waltham, MA, 3rd edn, 2011, vol. 3.
59 T. Hamada, S. Mizuno and H. Kitahata, *Soft Matter*, 2022, **18**, 9069–9075.
60 S. L. Veatch and S. L. Keller, *Biophys. J.*, 2003, **85**, 3074–3083.
61 A. Bekmurzayeva, W. J. Duncanson, H. S. Azevedo and D. Kanayeva, *Mater. Sci. Eng., C*, 2018, **93**, 1073–1089.